Amyloid β and the failure to form mitochondrial cristae. A biomimetic study involving artificial membranes

Nada Khalifat, Nicolas Puff, Mariam Dliaa, Miglena Angelova

Title:

Amyloid β and the failure to form mitochondrial cristae. A biomimetic study involving artificial membranes

Nada Khalifat [a], Nicolas Puff [b,c], Mariam Dliaa [a], Miglena I. Angelova [b,c *]

[a] UPMC Univ. Paris 06, UMR_S 938 CDR St Antoine, 75012 Paris, France

[b] UPMC Univ. Paris 06, UFR925 Physics Dept., 4 pl Jussieu, 75252 Paris, France

[c] Laboratoire Matière et Systèmes Complexes (MSC) CNRS UMR 7057, Univ. Paris Diderot - Paris 7, 75205 Paris, France

Running title:

Aβ and mitochondrial cristae. A biomimetic study…

[*] *Correspondence to:*

Miglena I. ANGELOVA, Prof. PhD

Laboratoire Matière et Systèmes Complexes (MSC) CNRS UMR 7057

University Paris Diderot - Paris 7

Bât. Condorcet, case 7056,

10 rue Alice Domon et Léonie Duquet

75205 Paris Cedex 13 - France

Tel : 00 33 1 57 27 70 82

Fax : 00 33 1 57 27 62 11

e-mail : miglena.anguelova@upmc.fr

Abstract**.** Alzheimer's disease (AD) is a degenerative disease of the central neural system which causes irreversible damage to neuron structure and function. The main hypothesis concerning the cause of AD is excessive accumulation of amyloid-β peptides (Aβ). There has been recently a surge in studies on neuronal morphological and functional pathologies related to Aβ-induced *mitochondrial* dysfunctions and morphological alternations. What is the relation between the accumulation of Aβ in mitochondria, decreased production of ATP, and the large number of mitochondria with broken or scarce *cristae* observed in AD patients' neurons? The problem is complex, as it is now widely recognized that mitochondria function determines mitochondrial inner membrane (IM) morphology and, conversely, that IM morphology can influence mitochondrial functions. In our previous work (Khalifat et al., Biophys J, 2008) we designed an artificial mitochondrial IM - a minimal model system (giant unilamellar vesicle, GUV) mimicking the IM. We showed experimentally that modulation of the local pH gradient at the membrane level of cardiolipin-containing vesicles induces dynamic membrane invaginations similar to the mitochondrial *cristae*. In the present work we show, using our artificial IM, that Aβ renders the membrane unable to support the formation of *cristae-like* structures when local pH gradient occurs, leading to the failure of this *cristae-like* morphology. Fluorescent probe studies suggest that the dramatic change of membrane mechanical properties is due to Aβ-induced lipid bilayer dehydration, increased ordering of lipids, loss of membrane fluidity, and possibly to Aβ-induced changes in dynamic friction between the two leaflets of the lipid membrane.

Keywords: Alzheimer's disease, mitochondria, amyloid-β (1-42) peptide (Aβ_{42}), biophysical phenomena, lipid bilayers, liposomes, pH gradient, videomicroscopy, micromanipulation, fluorescence polarization

INTRODUCTION

Mitochondria in Alzheimer's disease and the role of the amyloid-β peptide

Alzheimer's disease (AD) is a degenerative disease of the central neural system which causes massive neuronal loss, leading inevitably to progressive degeneration of mental capacities, and, ultimately, to death [1]. It is recognized that the progress of AD leads to morphological and functional neuronal pathologies at the extracellular as well at the intracellular level, both levels being non-exclusive and probably coupled [2, 3]. It is clear now that the increased level of *amyloid-β* (A*β*) peptide monomers, although not inherently harmful, leads to the formation of a diversity of A*β* aggregates (oligomers, proto-fibrils, fibrils) which are involved in a variety of pathological mechanisms when accumulating in the extra- and/or intracellular space of neurons. Recently, a surge in studies on AD-related neuronal pathologies focused on *Aβ-induced mitochondrial dysfunctions and morphological alterations* [4-10]. The present work examines these problems using, for the first time, a bio-mimetic artificial membrane approach.

The origin of intramitochondrial A*β* is far from certain [11]. The excessive production of A*β* peptide monomers results from the abnormal enzymatic cleavage of the amyloid-*β* protein precursor (A*β*PP) [12], a trans-membrane protein localized mainly in the cell membrane as well as in several intracellular sites, including the Golgi apparatus, endoplasmic reticulum, endosomal-lysosomal system and multivesicular bodies [2]. It is also possible that previously secreted A*β*, which forms the extracellular A*β* pool, could be taken up by cells and internalized into intracellular pools ([2] and articles cited therein). It is logical to presume that A*β* might gain access to the mitochondrial matrix by an intracellular trafficking mechanism with involvement of a specific transport mechanism on the mitochondrial membrane [10].

Furthermore, it was recently shown that Aβ can be imported from the cytoplasm into mitochondria *via* the translocase of the outer mitochondrial membrane (TOM) machinery [13]. The same study also demonstrated that Aβ accumulates in the mitochondrial *cristae* both in vivo and in vitro. However, with the recent localization of AβPP in mitochondial membrane fraction from brain of AD cases [14], the possibility of *in situ* Aβ production within mitochondria should be explored.

In comparison with normal specimens, mitochondria from AD patients show a larger variety of shapes and sizes as well as *altered cristae morphology*. A number of electron microscopy morphometric studies have shown *mitochondria with broken (disrupted) cristae* [15-17], see **Supplementary-Fig. 1B** and **Supplementary-Fig. 2**. Studies of AD cybrid cells proved they contained increased percentage of enlarged or swollen mitochondria that had a pale matrix and *scarce cristae* [16, 18]. Morphologies of " healthy" and "AD" mitochondria are shown in **Supplementary-Fig. 1A-1B,** respectively. It has been shown as well that in the case of AD some mitochondrial DNA (mtDNA) and some respiratory chain proteins, e.g. cytochrome oxidase-1, were present in the cytosol, instead of being, respectively, in the mitochondrial matrix and associated with the internal mitochondrial membrane [15]. On the other hand, the direct effect of Aβ on mitochondrial properties was further suggested by *in vitro* experiments in which cultured cells or isolated mitochondria were exposed to Aβ. Thus, it is now known that the Aβ accumulation in mitochondria promotes free radical generation and oxidative damage to all biomolecular types – DNA, RNA, proteins, lipids and sugars [19] **(**see as well S**upplementary-Fig. 3).** The altered enzymatic activity of proteins is the main result of the oxidative stress in which lipids play an important role in the terms of lipid peroxidation and the effect of the latter on protein structure and functions.

Surprisingly, the mechanisms relating the accumulation of Aβ in mitochondial *cristae* and matrix to the large number of mitochondria with broken and sparse *cristae* observed in

AD patients' neurons were not evoked. The problem is a challenging one, as it is now widely recognized that mitochondria function factors determine the inner membrane morphology and, conversely, that inner membrane morphology can influence mitochondrial functions [20-25] **(see as well Supplementary-Fig. 1C).** Indeed, it has been shown that *cristae* have a predominantly tubular nature, and, that the tubular structure of mitochondrial inner membrane is dynamic and coupled with the mitochondrial physiological state (in "healthy", as well as in "sick" mitochondria). Oxidative phosphorylation machinery proteins (electron transport chain proteins and ATP-synthase dimers) are located mostly in the *cristae* and the efficient work of this machinery, driven by acidity (pH) gradients, requires precise conditions regarding inner membrane tubular morphology.

What could be the factors that determine the failure of mitochondrial inner membrane morphology in the case of AD? Our hypothesis is the following: Aβ-induced alterations of *the purely physical properties of the lipid bilayer* could be the direct cause for this failure. We tested this hypothesis using artificial model system as described below.

Designing GUVs for the study of the dynamics of mitochondrial inner membrane morphology

In our previous work [26] we offered some original insights into the factors that determine the tubular structures of mitochondrial inner membrane *cristae*. In that study we designed a minimal IM model system, namely giant unilamellar vesicles (GUV) made of phosphatidylcholine (PC), phosphatidylethanolamine (PE), and cardiolipin (CL), PC /PE / CL 60:30:10 mol/mol. We showed experimentally (using micromanipulation and microinjection) that the modulation of local pH gradient at membrane level of cardiolipin-containing *lipid-only* vesicles induces dynamic tubular membrane invaginations (**Supplementary-Fig. 4,** and, **Supplementary Movie1_SF4).** These tubular dynamic structures were called *"cristae-like"*

as they mimic very well the mitochondrial IM morphology revealed by 3D electron microscopy (**Supplementary Fig. 1-C).** Our membrane model system helped reveal the inherent capacity of *cristae* morphology to become self-maintaining and to optimize ATP synthesis. Furthermore, our recent work [27] reported a chemically driven membrane shape instability (modulated by a source of pH gradient) that triggers the ejection of an exponentially-growing tubule. The instability is initiated by a dilation of the exposed outer leaflet which is coupled to the membrane spontaneous curvature and slowed down by intermonolayer friction. It is to note that the model, presented in details in [27] for the case of increasing local pH, is valid as well for the case of decreasing local pH (local acidification).

In the present work, we use again giant unilamellar vesicles (GUVs) as a biomimetic system in order to study the mitochondrial IM. This allowed us to perform direct real time visualization of morphological changes induced by the amyloid-β (1-42) (Aβ_{42}). We show that Aβ renders the membrane incapable of supporting the dynamics of tubular structure formation when a local pH gradient occurs, ultimately leading to *the failure of cristae-like dynamic morphology*. This is the case even when no problems were observed regarding membrane static behavior. In order to elucidate the molecular mechanisms underlying the failure of tubular structures formation, we carried out fluorescence studies of membrane properties involving Aβ_{42} interacting with artificial membranes mimicking the mitochondrial IM (designed as large unilamellar vesicles (LUVs)). The results suggest that dramatic changes in membrane dynamic properties at the scale of the entire GUV result from Aβ_{42}-induced membrane local dehydration, increased ordering of lipids, and loss of membrane fluidity. Aβ_{42}-induced changes in dynamic friction between the two leaflets of lipid membrane may take place as well.

MATERIALS AND METHODS

Reagents

Lipids were obtained and used without further purification as follows: egg yolk L-α-phosphatidylcholine (PC), Sigma; egg L-α-phosphatidylethanolamine (PE), heart bovine 1,3-bis(sn-3-phosphatidyl)-sn-glycerol diphosphatidylglycerol (cardiolipin, CL), brain porcine L-α-phosphatidylserine (PS), Avanti Polar Lipids. Fluorescent probes 6-propionyl-2-dimethylaminonaphthalene (Prodan), 6-dodecanoyl-2-dimethylaminonaphthalene (Laurdan) and 1,6-diphenyl-1,3,5-hexatriene (DPH) were from Molecular Probes Inc. Invitrogen ; Thiofavin T (ThT) - from Sigma. Amyloid-β (1 - 42) peptide (Aβ_{42}), synthetic, was from Sigma. Reversed peptide amyloid-β (42-1) (R-Aβ_{42}) was from Invitrogen (gift from Shi Du Yan, Columbia Univ. NY). EDTA and Dimethylsulfoxyde (DMSO) were from Sigma. HEPES – from Interchim.

Preparation of GUVs modeling the mitochondrial inner membrane (IM)

Giant unilamellar vesicles (GUVs) were formed from PC/PE/CL 60:30:10 mol/mol by the liposome electroformation method [28-30] in a thermostated chamber. The particular electroformation protocol established in [26]and used in this work was as follows: single lipids as well as lipid mixture solutions were prepared in chloroform/diethyl ether/methanol (2:7:1) at 1 mg/ml of total lipid. A droplet of lipid solution (1 µl) was deposited (avoiding sliding) on each of the two parallel platinum wires (diameter 0.8 mm, distance between axes 3 mm) and dried under vacuum for 15 min. An AC electrical field, 10 Hz, 0.26 V pp, was applied to the electrodes. Buffer solution (2 ml, pH 7.4, HEPES 0.5 mM, EDTA 0.5 mM,

temperature about 25°C) was added (avoiding agitation) to the working chamber. The voltage was gradually increased (over 2 h) up to 1 V pp and kept for 15 more minutes before switching the AC field off. The GUVs were ready for further utilization. In each preparation at least 10 GUVs of diameter 50 - 80 μm were available.

Imaging GUVs

We use a Zeiss Axiovert 200M microscope, equipped with a CDD camera (Cool SNAP HQ). The experiments were computer controlled using the Metamorph software (Roper Scientific).The morphological transformation and dynamics of the membrane were followed by phase contrast microscopy.

Microinjection

We made our micropipettes with internal diameter 0.3 μm, by pulling borosilicate glass capillaries using Narichige pipette puller PC-10. We used an Eppendorf FemtoJet for the local microinjection. The injection pressure was 15 - 25 hPa, and the initial distance from the GUV membrane – about 10 μm. The hydrodynamics of the solution injected by the micropipette could be visualized and thereby we could estimate that the part of the GUV membrane directly affected by the microinjection was about 10%. In fact, we aimed to locally modulate the proton concentration in order to create a *local* pH gradient at membrane level. Visualizing the flux from the micropipette also allowed us to estimate the dilution of the acid solution after injection. We calibrated the pH as a function of the dilution of 100 mM HCl pH 1.6 in the buffer in which the GUVs were formed (HEPES 0.5 mM, EDTA 0.5 mM, pH 7.4).

That allowed us to estimate the local pH value effectively created at the GUV membrane during the HCl delivery to be about pH 4 to 5.

Preparation of LUVs modeling the mitochondrial inner membrane (IM)

Large unilamellar vesicles (LUVs) were prepared using the extrusion method [31]. Samples were prepared by dissolving and mixing lipids PC/PE/CL 60:30:10 mol/mol in chloroform / methanol (9.4 : 0.6). Thereafter the solvent was removed under a stream of oxygen-free dry nitrogen (30 min). The residues were subsequently maintained under vacuum for 2 hours and then HEPES buffer, pH 7.4 (HEPES 5 mM, EDTA 0.1 mM) was added at room temperature (23°C) to yield a lipid concentration of 1 mM. The samples were heated at 30°C for 30 minutes, vortexed for 2 min and left in a sonication bath for 30 min, vortexed again for 1 min to ensure more uniform vesicle dispersion, and incubated again at 30°C for 15 min. The multilamellar vesicles were then extruded with a LiposoFast small-volume extruder equipped with polycarbonate filters (Avestin, Ottawa, Canada) as follows: 10 extrusions through 800 nm, and after that 21 extrusions through 100 nm filters. LUV average size was about 118 nm. The fluorescent probes (Prodan, Laurdan and DPH) were mixed with the lipids in the initial organic solution. We used the fluorescent probes at low concentrations in order not to perturbed the lipid bilayer native structure (1 fluorophore per 200 lipids in the case of Prodan and Laurdan, and 1 fluorophore per 500 lipids in the case of DPH). LUVs samples were kept at 4°C, and used for measurements the day after.

Spectrofluorimetry of LUVs

Steady-state fluorescence emission measurements were carried out using a Cary Eclipse Spectrofluorimeter equipped with polarizers and a thermostated cuvette holder (± 0.1°C).

Measurements of Prodan and Laurdan generalized polarization (GP) in relation with lipid bilayer order and hydration

Both fluorescent probes Prodan and Laurdan, [32, 33], contain the same fluorophore (dimethylaminonaphthalene) linked to a saturated acyl chain – propionyl (C_3) for Prodan and lauroyl (C_{12}) for Laurdan. The fluorescent naphthalene moiety of these probes possesses a dipole moment due to a partial charge separation between the 2-dimethylamino and the 6-carbonyl residues. Upon excitation, this dipole moment increases and may cause reorientation of surrounding solvent molecule dipoles. The energy spent for reorientation (dipolar relaxation) of solvent dipoles decreases the probe's excited state energy which is expressed in a continuous red shift of the probe's steady-state emission spectrum. Laurdan, due to its lauric acid tail, is tightly anchored in the hydrophobic core of phospholipid bilayers, with its fluorescent moiety residing at the level of the phospholipid glycerol back-bone. Prodan, however, with its shorter propionyl tail, is more loosely anchored in the bilayer. Consequently, it is located closer to the aqueous surface and is able to sense the more freely rotating water dipoles. The dipolar relaxation of water molecules surrounding phospholipid bilayers containing Prodan or Laurdan occurs in the lipid liquid-crystalline phase but not in the gel phase. That makes fluorescence emission maxima dependent on the phase state of the lipids: emission is blue (maximum emission I_{blue} at about 440 nm) in the gel phase and green (maximum emission I_{red} at about 490 nm) in the liquid-crystalline phase. The maximum of Prodan and Laurdan excitation for both gel and liquid-crystalline state is about 355 nm. The

*generalized polarization (**GP**) function* was defined as follows in order to describe the intermediate states of lipid membrane structure (states between pure gel and pure liquid-crystalline phase):

$$GP = \frac{I_{blue} - I_{red}}{I_{blue} + I_{red}} \quad ,$$

Thus, one has $GP = -1$ in pure liquid-crystalline, $GP = 1$ in pure gel phase membrane, and $-1 < GP < 1$ in any intermediate (or mixed) membrane states. Therefore, an increase in GP indicates, on average, a more ordered and less hydrated lipid membrane structure [33].

Measurements of DPH anisotropy (r_{DPH}) in relation with lipid bilayer fluidity

Fluorescent probes can be used to monitor the order and dynamics within the acyl chain region of liposome lipid bilayers [34]. One can study the DPH fluorescence anisotropy using excitation with polarized light. The excitation probability of a chromophore is proportional to $cos^2\theta$ where θ is the angle between the electric field vector of incident light $\vec{E}$ and electric absorption dipole moment of the chromophore. Therefore, the chromophore molecules with absorption dipole moment parallel to $\vec{E}$ will be excited with highest probability. The excitation of chromophore population by linearly polarized light leads to photo-selection (anisotropy) of excitation. Furthermore, the plane of polarization of the emitted light is not determined by the absorption dipole moment but by the transition dipole moment (which is generally not parallel to the absorption dipole moment), and the probability of emission of fluorescence with the plane of polarization at an angle Φ with respect to the transition dipole moment is proportional to $sin^2\Phi$. One should note that, even if the absorbers

were perfectly aligned with the plane of polarization of the exciting linearly polarized light $\vec{E}$, the emitted fluorescence will not be linearly polarized because of $sin^2\Phi$, a property called *fluorescence depolarization*. Many other factors can increase the extent of emitted fluorescence depolarization (in other words, can decrease the extent of fluorescence polarization, or, anisotropy); the most important one is the motion of the chromophore molecule. If the emitter is rotating very rapidly (e.g., due to the Brownian motion) so that there is a substantial change in orientation during the lifetime of the excited state, the fluorescence polarization (or, the fluorescence anisotropy) will be further reduced. This is an important phenomenon because the extent of this type of depolarization (or, fluorescence anisotropy loss) is affected by temperature, solvent viscosity, and the size and shape of the molecule containing the emitter. Conversely, a rise in anisotropy indicates increasing restrictions in orientation during the lifetime of the fluorophore excited state, and thereby, for example, for an increasing viscosity (decreasing fluidity) of the fluorescent probe's environment.

Fluorescence depolarization can be quantified, for example, by the term:

$$r = \frac{I_{VV} - GI_{VH}}{I_{VV} + 2GI_{VH}},$$

called fluorescence anisotropy (r). Here, I_{VV}, I_{VH}, I_{HV}, and I_{HH} are the fluorescence intensities measured for the corresponding orientations (V, vertical; H, horizontal) of the polarizer (the first index) and the analyzer (the second index) in our system. The sensitivity of the detection system for vertically and horizontally polarized light is taken into account by introducing the factor

$G = I_{HV} / I_{HH}$.

In this work we included DPH in our model lipid membranes and measured its fluorescence anisotropy (r_{DPH}) in order to study the effects of Aβ on lipid membrane fluidity as far as Aβ peptide interactions with lipid membrane might induce changes in lipid bilayer's structure, and thereby, change the extent of membrane hydration as well as its fluidity, as demonstrated in [35].

Preparation of Aβ_{42} *peptide and control solutions*

The Aβ stock solution (1 mg/ml ≈ 220 μM Aβ in DMSO): synthetic amyloid-β (1-42) peptide (Aβ_{42}) (commercially presented as a dry film at the bottom of the flask) was dissolved (at 1 mg/ml ≈ 220 μM, at least 12h before further use) in DMSO, an organic solvent efficient for keeping the peptide in monomeric form, as suggested in [36] (this stock Aβ-in-DMSO solution was kept at 4°C). *The buffer (0.5 mM HEPES, 0.5 mM EDTA, pH 7.4)*: adjusted to pH 7.4 with NaOH. *The Aβ buffer solution (0.05 mg/ml ≈ 11 μM Aβ peptide, 5 vol% DMSO, 0.5 mM HEPES, 0.5 mM EDTA, pH 7.4):* aliquots of the *Aβ stock solution* was diluted at 5:95 v/v in the buffer. *Control solution (5 vol% DMSO, 0.5 mM HEPES, 0.5 mM EDTA, pH 7.4):* DMSO was diluted at 5:95 v/v in *the buffer* to final DMSO concentration of 5 vol%.

Aβ_{42} *state of aggregation and fibril formation detection*

The process of Aβ monomer aggregation (sample "aging") starts as soon as the *Aβ buffer solution* is prepared from the stock (Aβ_{42} in DMSO) solution. It is known that the relative fraction of different size aggregates (monomers, oligomers, proto-fibrils, fibrils)

changes with the sample "age", ultimately giving a dominant fraction of large aggregates (fibrils) [37]. In particular, studies of the evolution of Aβ solutions under different physico-chemical conditions have shown that high peptide concentrations boost the aggregation process. **Moreover**, it is possible to reconstitute the effects of concentrations on the aggregation kinetics by the presence of various amounts of "seeds" (Aβ oligomers, proto-fibrils) in solutions of the freshly dissolved peptide [38]. Here we would like to stress that following simultaneously the kinetics of different size Aβ aggregates (monomers, oligomers, proto-fibrils, fibrils) proved to be a complicated technical task [37]. However, following only the kinetics of Aβ fibrils formation (*i. e.*, the aggregation final product) is possible using the classical (simple) method of Thioflavine T (ThT) fluorescence [37-40] which is also the method we have adopted in this study. The ThT bonds specifically to Aβ fibril aggregates but not to Aβ monomers neither to Aβ oligomers. The ThT, at concentrations above its $CMC_{ThT} \approx$ 4 μM, interacts with the β-sheets of Aβ fibril aggregates which leads to changes in ThT fluorescence, thus offering a means of studying the kinetics of Aβ aggregation to fibrils. (Note that the ThT does not interact with Aβ fibrils at pH ≤ 5, as both species are positively charged at that pH range.)

ThT fluorescence is characterized by two types of spectra: (i) the characteristic spectrum of *free ThT* in aqueous solution (in absence of Aβ fibrils) with $\lambda_{ex}/\lambda_{em}$ *330/445 nm*; (ii) the characteristic spectrum of *ThT linked to Aβ fibrils* (in presence of Aβ fibrils) with $\lambda_{ex}/\lambda_{em}$ *450/482 nm* [37, 40, 41]. In order to study the kinetics of Aβ fibrils formation, we added (at given times) aliquots of the Aβ_{42} buffer solution to ThT aqueous solutions (ThT 35 μM, 270 μl, at 25°C) and checked for the characteristic fluorescence of the two states of ThT fluorophores presented in the medium: the *free* ThT , and, the ThT *linked* to Aβ fibrils. Thus, we always measured the total ThT fluorescence in the three cases: in the *Aβ buffer solution*

(11 μM Aβ_{42} peptide, 5 vol% DMSO, 0.5 mM HEPES, 0.5 mM EDTA, pH 7.4), in the *control solution* (5 vol% DMSO, 0.5 mM HEPES, 0.5 mM EDTA, pH 7.4), and, in the *buffer* (0.5 mM HEPES, 0.5 mM EDTA, pH 7.4). The variation of *linked* ThT emission ($\lambda_{ex}/\lambda_{em}$ *450/482 nm*) as a function of time (given in relative units as emission intensity of ThT in the *Aβ buffer solution* / ThT in *the control solution*) represents the kinetics of Aβ fibrils formation.

RESULTS

Aβ_{42} induces failure of GUVs cristae-like morphology

Fig. 1 represents the kinetics of Aβ_{42} fibrils formation using the data shown in **Supplementary-Fig. 5** where the total ThT fluorescence for a sample of an Aβ_{42} buffer solution is presented after aging 4h, 22h, 47, and 95h, respectively (as described in *Materials and Methods*). Fibril formation proved to be fast under the given conditions (11 μM Aβ_{42} peptide, 5 vol% DMSO, 0.5 mM HEPES, 0.5 mM EDTA, pH 7.4, T=25°C)**;** practically no lag time was observed. This result suggests the possible presence of "seeds" (Aβ_{42} oligomers) in the initial Aβ buffer solution, according to [42]. Fibril formation reaches saturation at an "age" of ~ 40h in our peptide buffer solution. The dashed lines indicate the state of the two kinds of Aβ_{42} buffer solutions (aged about 1h, and about 48h, respectively) used in this work for studying Aβ_{42} peptide interactions with model membranes. According to previous studies [37], one can conclude that the *Aβ_{42} peptide was present mainly in fibrils at saturation in our Aβ_{42} buffer solutions aged 48h (henceforth referred to as "aged" Aβ), while the fibrils were*

still rare (a dominating fraction of monomers, oligomers and some protofibrils) in the Aβ_{42} buffer solutions aged 1h (henceforth referred to as "fresh" Aβ).

Our GUVs (modeling the mitochondrial inner membrane leaflet which is exposed to cytoplasmic pH) were prepared from PC /PE / CL 60:30:10 mol/mol in buffer at pH 7.4 by the electroformation method [28] and observed directly using optical video microscopy system. We started the study of Aβ_{42} / membrane interactions by adding locally at the GUV exterior Aβ_{42} buffer solution (using a micro-pipette, injection time $\approx$ 40 min) and observing the resulting GUV behavior during the following 2h. We then induced local acidification (adding locally by a micro-pipette, outside the GUV, 10 to 100 mM HCl solutions) in order to test the capacity of this GUV to develop the characteristic *cristae-like* morphology. Tests were carried out in a manner similar to our experiments studying the dynamics of mitochondrial IM morphology described in the introduction as well as in [26], and illustrated in **Supplementary-Fig. 4 (Supplementary Movie1 – SF4)**. In this manner, we tested the capacity of GUVs, pretreated with either "aged" or "fresh" Aβ_{42} buffer solution, to develop the characteristic dynamic *cristae-like* morphology.

The capacity of the GUV (pretreated with Aβ_{42} peptide) to develop *cristae-like* morphology failed in both cases, but in a different manner, as described below. That was probably due to different underlying mechanisms, as we shall discuss further.

(i) The case of "aged" Aβ. **Fig. 2** and **Supplementary Movie2_F2** present GUV mimicking the internal mitochondrial membrane being treated locally with an "aged" Aβ_{42} buffer solution. A peptide-induced increase of membrane thermal fluctuations indicated a lowering of GUV global membrane tension which can be due to increasing GUV excess area. The vesicle shape changed from quasi-spherical (frame: 0s) to flaccid (frame: 390s). No visible changes were observed further up to about 40 min treatment with the Aβ solution. No membrane local deformation was observed. The vesicle preserved its integrity, and no visible

membrane damage occurred. The Aβ fibrils can associate initially with the GUV membrane by electrostatic interactions (the protein and the membrane exhibiting positive and negative surface potentials, respectively, at pH 7.4), as suggested in [43, 44]. After this electrostatic adsorption, a partial penetration of the fibril's hydrophobic face into the lipid bilayer takes place [44] as indicated by the increase in membrane thermal fluctuations. Next, we tested the capacity of this GUV to develop *cristae-like* morphology upon local acidification (see **Fig. 3** and **Supplementary Movie3_F3)**. The local acidification (adding 10mM HCl by micropipette) initiated local membrane deformation (frame: 4.7s) followed by brutal macroscopic rupture of the membrane zone affected by the acid (frame: 5.2s), and explosion of the GUV (frame: 6s). When acid addition was stopped, the damaged membrane zone "healed", forming a kind of "scar" (dense clumps), (frame: 46.5s). No *cristae-like* morphology was developed.

We interpret the observed brutal membrane rupture as isoelectric precipitation upon the local acidification of the Aβ fibrils previously associated with the GUV membrane. Indeed, it was shown that upon acidification Aβ is susceptible to isoelectric precipitation when the peptide is near to its pI of 5.5 [45]. In such a case, a greater fraction of peptide is converted into a "mat" of amorphous filamentous aggregates having hydrophobic surfaces and agglomerating into insoluble structures, being distinctly different from fibrils formed at pH 7 to 8 [45, 46]. Regarding our experiment, such hydrophobic amorphous Aβ aggregates probably form on the membrane upon the local acidification, and, instantaneously**,** they try to **occupy** the hydrocarbon core (hydrophobic aliphatic chains) of lipid bilayer, destabilizing it, and, inducing catastrophic consequences for the membrane integrity.

(ii) The case of "fresh" Aβ. **Fig. 4** and **Supplementary Movie4 _F4** present a GUV mimicking the internal mitochondrial membrane being treated locally with "fresh" Aβ_{42} buffer solution. In the beginning, vesicle size (frame: 0s) slightly decreased (frame: 193.3s).

No visible further changes were observed up to about 40 min treatment with the Aβ solution. Like in the case of treatment with "aged" Aβ buffer solution (**Fig. 2**), no local membrane deformation was observed, the vesicle preserved its integrity, and no visible membrane damage occurred. We next tested the capacity of this GUV to develop *cristae-like* morphology upon local acidification (see **Fig. 5** and **Supplementary Movie5 _F5)**. The local acidification (with up to 100 mM HCl) induced no visible effects to the GUV membrane, in contrast with the brutal rupture (achieved when adding HCl solution of only 10 mM), observed in the case of acidification, after treatment with "aged" Aβ **(Fig. 3)**. Nevertheless no visible membrane damage occurred, and the local acidification of GUV pre-treated with "fresh" Aβ_{42} did not induce any local membrane invagination. No *cristae-like* morphology was developed, in contrast ton the case of local acidification of the control "healthy" GUV (all other parameters being equal).

We suggest that, in the case of "fresh" Aβ pretreatment, the membrane shape becomes "inert" with respect to creation of local pH gradient because of formation of microscopic (molecular scale) pores due to small Aβ_{42} aggregates (Aβ_{42} oligomers) insertion into the lipid bilayer. The proton gradient, induced by the local addition of acid solution, might rapidly dissipate across the membrane due to the presence of these pores without any macroscopic (vesicle scale) damage. The possibility of small ion channels formation in the case of "fresh" Aβ_{42} is supported by the results presented in [47-49]. The experimental procedures described therein show that the interaction of Aβ with a variety of membranes, both artificial and natural, results in the subsequent formation of Aβ ion channels. Moreover, molecular dynamics modeling results support as well the hypothesis that small Aβ oligomers can form ion channels in model membranes [50, 51].

The similarity between the "aged" Aβ_{42} induced failure of GUV *cristae-like* morphology, and the morphological features coupled with mitochondrial dysfunctions in AD presented in the Introduction (mitochondria with broken, disrupted, or scarce *cristae*), is striking. It may possibly be due to similar Aβ induced changes to the molecular structure and the physical properties of the lipid membrane. This made us extend our artificial membrane study as presented in the next part.

Aβ_{42} fibrils induce lipid bilayer dehydration and decreasing membrane fluidity to LUVs that model mitochondrial inner membrane

The transverse profile of the lipid bilayer represents a complex environment of decreasing polarity starting from the polar lipid heads, through the glycerol moieties, and down to the furthest extent of the hydrophobic aliphatic chains. Water molecules penetrate into the lipid to a certain extent depending on lipid molecule organization which can be more or less ordered [32, 33]. The structure of the lipid bilayer is linked, in particular, to its fluidity (or, viscosity) [34]. Aβ peptide interactions with the lipid membrane might induce changes in the lipid bilayer structure, thereby changing the extent of its hydration and its fluidity [35]. Here we present our exploration of microscopic (molecular level) effects induced by "*aged" Aβ_{42} buffer solutions* on LUVs (PC / PE / CL 60:30:10 mol/mol) modeling the mitochondrial inner membrane and containing lipophilic fluorescent probe (Prodan, Laurdan, or, DPH). These fluorescent molecules localize at different depths in the lipid bilayer, thereby yielding information on the lipid membrane's global properties, as explained in the *Materials and Methods*.

We present below fluorescence spectra properties of Prodan as well as those of Laurdan in terms of generalized polarization (*GP*). The effects of Aβ_{42} peptide induced at the

level of polar lipid heads (GP_{PRODAN}), and at the level of glycerol moieties ($GP_{LAURDAN}$) are presented in **Fig. 6 A, B.** We studied generalized polarizations for different total peptide / lipid ratios (0; 1/100, 2/100, and 4.4/100 mol/mol). One can see that, in absence of Aβ_{42} peptide, as well as for Aβ_{42} of low concentrations, the *GP*s were practically constant or slightly rising with time (at least up to 4h), **Fig. 6 A-left, B-left**. In any case, the higher the peptide / lipid ratio was, the faster the GP increase over time. For example, after 4h incubation at a peptide / lipid ratio of 4.4/100 mol/mol, the GP_{PRODAN} increased from -0.18 (t = 0h) to -0.05 (t = 4h), and the $GP_{LAURDAN}$ increased from +0.015 (t = 0h) to +0.057 (t = 4h). Recall that an increase of GP indicates a more ordered and less hydrated lipid membrane structure [32, 33]. After kinetics measurements (lasting 4h), we gradually lowered the pH of the Aβ_{42}-LUV samples by adding aliquots of acid solution (100 mM HCl), **Fig. 6 A-right, B-right**. The GPs of both probes were rising when pH was decreasing. The pH effect was stronger at higher peptide/lipid ratio. For example, at peptide/lipid ratio 2/100 mol/mol, the GP_{PRODAN} raised from -0.15 (pH 7.4) to +0.13 (pH 3), and the $GP_{LAURDAN}$ raised from +0.01 (pH 7.4) to +0.26 (pH 3). Our experiments involving Prodan and Laurdan fluorescence reveal that increasing the total peptide/lipid ratio of Aβ_{42} fibrils, as well as decreasing the pH of the medium, lead to dehydration and increasing apolarity (structuring) close to the water/lipid interface of lipid bilayers modeling the mitochondrial inner membrane. The pH effect was stronger at higher peptide/lipid ratios. **Fig. 6 C** presents the anisotropy of DPH (r_{DPH}), giving information about membrane hydrophobic core fluidity. Adding Aβ_{42} to the LUV suspension induced a gradual increase in DPH anisotropy with the time, **Fig. 6 C-left.** The vesicle membrane becomes more viscous (less fluid) due to its interaction with the peptide, the later being predominantly presented as fibrils in our "aged" peptide solution. The effect is stronger at higher peptide/lipid ratios. After kinetic measurements (lasting 4h), we gradually lowered the pH of the Aβ-LUV samples by adding aliquots of acid solution (100 mM HCl), **Fig. 6 C-**

right. The gradual decrease of bulk pH induces a gradual increase in DPH anisotropy. The rise of r_{DPH} was stronger for higher peptide to lipid ratios. For example, at total peptide to lipid ratio of 4.4/100 mol/mol, r_{DPH} increases from +0.15 (t = 0h) to +0.26 (t = 4h), and, from +0.26 (pH 7.4) to +0.30 (pH 3). Recall that the more viscous the lipid bilayer**,** the less mobile the fluorescent probe**,** and the higher the anisotropy**,** as explained in the *Materials and Methods*. These results suggest that the DPH molecular motion is restricted by the increased order of the lipid fatty acid chains.

These results are coherent with several previous findings. Indeed, some studies regarding the effect of Aβ aggregation state on the membrane fluidity, assessed by monitoring the anisotropy of DPH [35, 52] embedded in model membranes (POPC, POPG, POPC/POPE/POPS/Chol (36:36:10:18 w/w), and, POPC/POPE/POPS/Chol/gangliosides (33:33:10:16:8 w/w)), reported that aggregated, but not monomeric, Aβ at pH 7 induced decreases in membrane fluidity in all types of liposome preparations investigated. Apart from the studies of Aβ interactions with model membranes, reduction of Aβ induced membrane fluidity was found in human cortex [53] membranes. Aβ_{40} decreases the fluidity of mouse brain membranes in a concentration-dependent fashion [54]. On the other hand, the generalized polarization of Laurdan measurements [52] in *non-CL containing* lipid membranes led authors to conclude that Aβ induced little to no change in membrane structure or water penetration near the bilayer surface. In contrast, our experiments involving Prodan and Laurdan fluorescence in *CL containing* lipid bilayers modeling mitochondrial inner membrane (PC/PE/CL 60:30:10 mol/mol) reveal that increasing the total peptide to lipid ratio of Aβ fibrils, as well as lowering the pH of the medium, lead to progressive dehydration and increasing apolarity (structuring) close to the water/lipid interface. This is compatible with [43] which reported that the fibrillation of Aβ was found to be increased significantly in the presence of anionic phospholipids i.e., PA, PS, CL and PIs (PI, PIP, PIP2). The effect on Aβ

fibrillation was dependent on the number of phosphate groups in the phosphoinositides (note that the CL has 2 phosphate groups).

The failure of GUVs cristae-like morphology is induced specifically by the Aβ_{42}

We carried out control experiments, using the reversed peptide R-Aβ_{42} (amyloid-β (42-1)), in order to check the specificity of Aβ_{42} to induce failure of the cristae-like morphology. Under the same experimental conditions, we tested the capacity of a GUV (pre-treated with either "aged", or, "fresh" R-Aβ_{42} buffer solution) to develop *cristae-like* morphology upon local acidification. The GUVs, upon subsequent local acidification, maintained their capacity to develop cristae-like tubular invaginations similar to those of the "healthy" (not pre-treated with any Aβ) GUV. However, the profile and the dynamics of the pH-induced membrane structures was different. So, in the case of "aged" R-Aβ (**Fig. 7 and Supplementary Movie6_F7)** the pH-induced tubular structures were thicker, shorter and less dynamic compared to those of "healthy" GUVs, while in the case of "fresh" R-Aβ (**Fig. 8 and Supplementary Movie7_F8)** the initial tubular structures fragmented rapidly giving endocytic vesicles (non-reversible process). This indicates that the R-Aβ_{42} interacts with the GUV membrane but does not have the specific "fatal toxicity" impact on the *cristae-like* morphology as the native peptide (the Aβ_{42}) does.

It is interesting to note that the findings presented recently in [55] demonstrate that even at low concentrations, Aβ_{42}, as compared with the reversed peptide R-Aβ_{42}, significantly impairs synaptic mitochondrial distribution and axonal mitochondrial mobility and, in addition, induces changes in mitochondrial morphology involving increased axonal mitochondrial fragmentation.

DISCUSSION

When developing our model systems, we aimed to mimic the following scenario: the $A\beta_{42}$ peptide, as presented in cytosol at pH 7.4, attains the mitochondrial inner membrane. When local acidification starts, as a result of the work of electron transport chain proteins, the inner membrane *cristae* should normally develop. Our task was to investigate, by means of our artificial model system, whether the peptide might thwart the dynamics of the characteristic *cristae-like* membrane deformation. We took into account that the interaction of $A\beta$ peptide with the membrane might depend on peptide aggregation state [35, 44] as well as on the local pH and temperature [38], and, that the $A\beta$ aggregation and interaction with the membrane might be specifically catalyzed by the lipid bilayer [56-59]. One should emphasize that the state of aggregation of $A\beta$ at the level of mitochondrial inner membrane in *biological* samples is still very difficult to determine because of the extremely low $A\beta$ concentrations in this case. Additionally no experimental method exists so far for revealing the state of $A\beta$ aggregation directly on the IM of unique mitochondria. The advantage of our biomimetic experiments is that the effects of $A\beta$ solutions on lipid bilayer properties and membrane shape transformations can be directly visualized and studied in both cases of fibril ("aged") as well as oligomer ("fresh") $A\beta$.

In the above framework, we have shown that $A\beta$ interaction with lipid bilayers mimicking the mitochondrial IM may take place without macroscopic (vesicle scale) membrane damage. Notwithstanding this "peaceful" (at first sight) association of the peptide with the lipid membrane, the $A\beta$ thwarted the formation of *cristae-like* membrane structures upon later local acidification. Interestingly, the failure of the dynamics of *cristae-like* deformations happened in a different manner depending on whether the membrane was pre-treated with "aged" or with "fresh" $A\beta$ solution. In the first case macroscopic the membrane

was brutally ruptured as soon as membrane tubular deformation started, while in the second case no membrane deformation was initiated. The rupture of cristae-like tubules, due to pretreatment with "aged" (fibril containing) Aβ solution, was remarkably similar to the morphological features coupled with mitochondrial dysfunctions in Alzheimer's disease: *mitochondria with broken (disrupted) cristae* [15-17] (see **Supplementary-Figure 2)**, and mitochondria with a pale matrix and *scarce cristae* [16, 18] (see **Supplementary-Fig. 1B)**.

We think that the remarkable potency of "aged" Aβ_{42} to induce mechanical damage (harsh disruption) of a GUV, when fast membrane shape transformation is driven by the local acidification **(Fig. 3),** might be explained by the combination of: (i) the strong capacity of Aβ_{42} *fibrils* to *rigidify* the lipid membrane, as fibrils dehydrate the membrane and decrease its fluidity, (ii) the specificity of Aβ_{42} fibrils / membrane interactions due to the *presence of CL in the lipid bilayer*, and, (iii) the *mechanical stress* imposed to the membrane due to fast isoelectric precipitation of membrane surface bound Aβ_{42} fibrils, leading to peptide sinking into the membrane hydrophobic core. We would like to point out that, in terms of "Material Science and Membrane Mechanics", the combination of *rigidity* and *stress* leads to *integrity failure*.

In the case of pre-treatment with "fresh" Aβ_{42}, our results reveal a different mechanism for inducing failure to create a *cristae*-like morphology where no membrane deformation was initiated upon a subsequent local acidification. We could explain the observed lack of membrane shape "response" to the pH gradient by the possibility that small Aβ_{42} aggregates (Aβ_{42} oligomers) insert into the lipid bilayer and form microscopic (molecular scale) pores in this case. The proton gradient, induced by the local addition of acid solution, may rapidly dissipate across the membrane due to the presence of these pores without any occurrence of macroscopic (vesicle scale) membrane event. A direct test for Aβ-induced ion channels formation in our GUVs might be designed using patch-clamp

techniques, similar to electrophysiological tests performed, *e.g.*, in [60]. The practical realization of this task however demands careful consideration in adapting our artificial membrane system to the specific ionic conditions for patch-clamp recordings.

Finally, no matter the predominant presence of Aβ_{42} fibrils and / or Aβ_{42} oligomers, the result regarding our model membrane was essentially the same: the lipid membrane failed to develop *cristae*-like morphology upon local acidification. The failure of GUVs cristae-like morphology was induced specifically by the Aβ_{42} since we demonstrated that neither the "aged" nor the "fresh" reversed peptide (R-Aβ_{42}) abolished the membrane capacity to develop *cristae*-like tubular invaginations. At the same time the profile and the dynamics of the pH-induced membrane structures in the case of pretreatment with R-Aβ_{42} was different from those of the "healthy" GUV. After all, it is not surprising that adding an amphiphilic peptide to the membrane would affect somehow the membrane; the point however is "what is the specific effect?". Our control experiments with the reversed protein R-Aβ_{42} clearly show the beta-amyloid inhibition of *cristae*-like structures has a significant degree of sequence and structure specificity.

Our work puts forward several *new ideas which might be biologically relevant*.

First, the Aβ fibril aggregates might change *directly* (without lipid biochemical degradation) the global physical properties of the mitochondrial inner membrane by decreasing membrane core fluidity, inducing lipid bilayer dehydration and increasing apolarity (structuring) close to the water/lipid interface of the lipid bilayer. Of course, the oxidative stress related to the specific function of the mitochondrial IM and the related lipid biochemical degradation (lipid peroxidation) enhance these lipid-based effects. It is interesting to point out in this context that significant reduction of membrane fluidity in membranes of mitochondria extracted from different areas of AD brains was reported in [61].

The authors' explanation was that this might be caused by a greater lipid peroxidation of biological membranes.

Second, we suggest that changes in lipid bilayer *physical* properties induced by Aβ fibrils may play *a special direct role in* membrane functions involving rapid *membrane shape changes*, this being typically the case of the mitochondrial inner membrane. In fact, the membrane, being "normally" visco-elastic, becomes more viscous then elastic and loses its capacity to respond quickly to the mechanical constraint imposed by local acidification. The direct consequence of these alternations could be a harsh membrane rupture due to the rapid membrane shape changes driven by local acidification.

Third, Aβ oligomers might insert themselves into the lipid bilayer and form pores (ion channels) in the mitochondrial inner membrane. These pores can have dramatic consequences regarding mitochondrial functions**:** decreased mitochondrial trans-membrane potential, decreased capacity to accumulate calcium, and uncoupling of respiration [62, 63].

CONCLUSION

The mechanisms affecting mitochondria in AD remain controversial: any deterioration of mitochondrial functions may cause neuronal deficiency. Our biomimetic studies involving artificial membranes encourage us to put forward an original hypothesis regarding mitochondria deficiency and Alzheimer's disease: AD might be a consequence of the failure of fundamental physical, *purely mechanical* properties of the mitochondrial inner membrane. We will call the specific Aβ toxicity in this case *"mechanical toxicity"*. Thus, Aβ induced "mechanical toxicity" could lead to a membrane inability to support the shape dynamics underlying, and inherent to, normal functioning of the mitochondrial inner membrane.

In addition, Aβ–fibril induced membrane dehydration, ordering, and increased membrane viscosity might cause membrane protein malfunctions, thereby contributing *indirectly* to the insufficiency of respiratory chain protein functions and ATP synthesis. On the other hand, Aβ oligomers might induce ion channels formation, compromising the driving force behind the characteristic tubular *cristae* morphology, abolishing mitochondrial transmembrane potential, decreasing the capacity to accumulate calcium, and uncoupling respiration.

ACKNOWLEDGEMENTS

We thank Shi Du Yan (Columbia Univ. NY) for the gift of R-Aβ peptide as well as for the fruitful discussions, suggestions and criticism. We thank Todor Tochev and Fred Menger (Emory Univ., Atlanta) for proof reading. This work was supported by the UPMC / FED 21 project.

REFERENCES

[1] Mattson MP (2004) Pathways towards and away from Alzheimer's disease. *Nature* **430**, 631-639.

[2] LaFerla FM, Green KN, Oddo S (2007) Intracellular amyloid-β in Alzheimer's disease. *Nat Rev Neurosci* **8**, 499-509.

[3] Wirths O, Multhaup G, Bayer TA (2004) A modified β-amyloid hypothesis: intraneuronal accumulation of the β-amyloid peptide - the first step of a fatal cascade. *Journal of Neurochemistry* **91**, 513-520.

[4] Swerdlow RH, Burns JM, Khan SM (2010) The Alzheimer's disease mitochondrial cascade hypothesis. *J Alzheimers Dis* **20 Suppl 2**, S265-279.

[5] Swerdlow RH, Khan SM (2004) A "mitochondrial cascade hypothesis" for sporadic Alzheimer's disease. *Med Hypotheses* **63**, 8-20.

[6] Castellani R, Hirai K, Aliev G, Drew KL, Nunomura A, Takeda A, Cash AD, Obrenovich ME, Perry G, Smith MA (2002) Role of mitochondrial dysfunction in Alzheimer's disease. *Journal of Neuroscience Research* **70**, 357-360.

[7] Manczak M, Anekonda TS, Henson E, Park BS, Quinn J, Reddy PH (2006) Mitochondria are a direct site of Aβ accumulation in Alzheimer's disease neurons: implications for free radical generation and oxidative damage in disease progression. *Hum. Mol. Genet.* **15**, 1437-1449.

[8] Reddy PH, Beal MF (2008) Amyloid beta, mitochondrial dysfunction and synaptic damage: implications for cognitive decline in aging and Alzheimer's disease. *Trends in Molecular Medicine* **14**, 45-53.

[9] Caspersen C, Wang N, Yao J, Sosunov A, Chen X, Lustbader JW, Xu HW, Stern D, McKhann G, Yan SD (2005) Mitochondrial Aβ: a potential focal point for neuronal metabolic dysfunction in Alzheimer's disease. *Faseb J* **19**, 2040-2041.

[10] Chen JX, Yan SS (2010) Role of Mitochondrial Amyloid-beta in Alzheimer's Disease. *J Alzheimers Dis* **20 Suppl 2**, 569-578.

[11] Chen JX, Yan SD (2007) Amyloid-beta-induced mitochondrial dysfunction. *J Alzheimers Dis* **12**, 177-184.

[12] Hardy J, Selkoe DJ (2002) The Amyloid Hypothesis of Alzheimer's Disease: Progress and Problems on the Road to Therapeutics. *Science* **297**, 353-356.

[13] Hansson Petersen CA, Alikhani N, Behbahani H, Wiehager B, Pavlov PF, Alafuzoff I, Leinonen V, Ito A, Winblad B, Glaser E, Ankarcrona M (2008) The amyloid β-

peptide is imported into mitochondria via the TOM import machinery and localized to mitochondrial cristae. *Proceedings of the National Academy of Sciences* **105**, 13145-13150.

[14] Yamaguchi H, Yamazaki T, Ishiguro K, Shoji M, Nakazato Y, Hirai S (1992) Ultrastructural localization of Alzheimer amyloid beta/A4 protein precursor in the cytoplasm of neurons and senile plaque-associated astrocytes. *Acta Neuropathol* **85**, 15-22.

[15] Hirai K, Aliev G, Nunomura A, Fujioka H, Russell RL, Atwood CS, Johnson AB, Kress Y, Vinters HV, Tabaton M, Shimohama S, Cash AD, Siedlak SL, Harris PLR, Jones PK, Petersen RB, Perry G, Smith MA (2001) Mitochondrial Abnormalities in Alzheimer's Disease. *J. Neurosci.* **21**, 3017-3023.

[16] Baloyannis SJ, Costa V, Michmizos D (2004) Mitochondrial alterations in Alzheimer's disease. *American Journal of Alzheimer's Disease and Other Dementias* **19**, 89-93.

[17] Baloyannis SJ (2006) Mitochondrial alterations in Alzheimer's disease. *J Alzheimers Dis* **9**, 119-126.

[18] Trimmer PA, Swerdlow RH, Parks JK, Keeney P, Bennett JP, Miller SW, Davis RE, Parker WD (2000) Abnormal Mitochondrial Morphology in Sporadic Parkinson's and Alzheimer's Disease Cybrid Cell Lines. *Experimental Neurology* **162**, 37-50.

[19] Sayre LM, Perry G, Smith MA (2008) Oxidative Stress and Neurotoxicity. *Chemical Research in Toxicology* **21**, 172-188.

[20] Lea PJ, Temkin RJ, Freeman KB, Mitchell GA, Robinson BH (1994) Variations in mitochondrial ultrastructure and dynamics observed by high resolution scanning electron microscopy (HRSEM). *Microsc. Res. Tech.* **27**, 269-277.

[21] Logan DC (2006) The mitochondrial compartment. *J. Exp. Bot.* **57**, 1225-1243.

[22] Mannella CA, Marko M, Penczek P, Barnard D, Frank J (1994) The internal compartmentation of rat-liver mitochondria: Tomographic study using the high-voltage transmission electron microscope. *Microsc. Res. Tech.* **27**, 278-283.

[23] Mannella CA, Pfeiffer DR, Bradshaw PC, Moraru II, Slepchenko B, Loew LM, Hsieh CE, Buttle K, Marko M (2001) Topology of the mitochondrial inner membrane: dynamics and bioenergetic implications. *IUBMB Life* **52**, 93-100.

[24] Mannella CA (2006) The relevance of mitochondrial membrane topology to mitochondrial function. *Biochim. Biophys. Acta* **1762**, 140-147.

[25] Mannella CA (2006) Structure and dynamics of the mitochondrial inner membrane cristae. *Biochim. Biophys. Acta* **1763**, 542-548.

[26] Khalifat N, Puff N, Bonneau S, Fournier JB, Angelova MI (2008) Membrane deformation under local pH gradient: mimicking mitochondrial cristae dynamics. *Biophys J* **95**, 4924-4933.

[27] Fournier JB, Khalifat N, Puff N, Angelova MI (2009) Chemically triggered ejection of membrane tubules controlled by intermonolayer friction. *Phys Rev Lett* **102**, 018102.

[28] Angelova MI, Dimitrov DS (1986) Liposome electroformation. *Faraday Discuss. Chem. Soc.* **81**, 303-311; discussion 345-349.

[29] Angelova MI, Dimitrov DS (1988) A mechanism of liposome electroformation. *Prog. Colloid Polym. Sci.* **76**, 59-67.

[30] Angelova MI, Soléau S, Méléard P, Faucon J-F, Bothorel P (1992) AC field controlled formation of giant fluctuating vesicles and bending elasticity measurements. *Springer Proc. Physics* **66**, 178-182.

[31] MacDonald RC, MacDonald RI, Menco BPM, Takeshita K, Subbarao NK, Hu L-r (1991) Small-volume extrusion apparatus for preparation of large, unilamellar vesicles. *Biochimica et Biophysica Acta (BBA) - Biomembranes* **1061**, 297-303.

[32] Krasnowska EK, Gratton E, Parasassi T (1998) Prodan as a Membrane Surface Fluorescence Probe: Partitioning between Water and Phospholipid Phases. *Biophysical journal* **74**, 1984-1993.

[33] Parasassi T, Krasnowska EK, Bagatolli L, Gratton E (1998) Laurdan and Prodan as Polarity-Sensitive Fluorescent Membrane Probes. *Journal of Fluorescence* **08**, 365-373.

[34] Lentz BR (1993) Use of fluorescent probes to monitor molecular order and motions within liposome bilayers. *Chemistry and Physics of Lipids* **64**, 99-116.

[35] Kremer JJ, Pallitto MM, Sklansky DJ, Murphy RM (2000) Correlation of β-Amyloid Aggregate Size and Hydrophobicity with Decreased Bilayer Fluidity of Model Membranes *Biochemistry* **39**, 10309-10318.

[36] Ege C, Lee KYC (2004) Insertion of Alzheimer's A-beta 40 Peptide into Lipid Monolayers. *Biophys. J.* **87**, 1732-1740.

[37] Benseny-Cases N, Cócera M, Cladera J (2007) Conversion of non-fibrillar beta-sheet oligomers into amyloid fibrils in Alzheimer's disease amyloid peptide aggregation. *Biochemical and Biophysical Research Communications* **361**, 916-921.

[38] Hortschansky P, Schroeckh V, Christopeit T, Zandomeneghi G, Fändrich M (2005) The aggregation kinetics of Alzheimer's β-amyloid peptide is controlled by stochastic nucleation. *Protein Science* **14**, 1753-1759.

[39] Khurana R, Coleman C, Ionescu-Zanetti C, Carter SA, Krishna V, Grover RK, Roy R, Singh S (2005) Mechanism of thioflavin T binding to amyloid fibrils. *Journal of Structural Biology* **151**, 229-238.

[40] Levine H, III (1993) Thioflavine T interaction with synthetic Alzheimer's disease beta-amyloid peptides: Detection of amyloid aggregation in solution. *Protein Science* **2**, 404-410.

[41] Levine H (1997) Stopped-Flow Kinetics Reveal Multiple Phases of Thioflavin T Binding to Alzheimer β (1-40) Amyloid Fibrils. *Archives of Biochemistry and Biophysics* **342**, 306-316.

[42] Jarrett JT, Berger EP, Lansbury PT (1993) The carboxy terminus of the β amyloid protein is critical for the seeding of amyloid formation: Implications for the pathogenesis of Alzheimer's disease. *Biochemistry* **32**, 4693-4697.

[43] Chauhan A, Ray I, Chauhan VPS (2000) Interaction of amyloid beta-protein with anionic phospholipids: possible involvement of Lys28 and C-terminus aliphatic amino acids. *Neurochemical Research* **25**, 423-429.

[44] Bokvist M, Lindström F, Watts A, Gröbner G (2004) Two Types of Alzheimer's β-Amyloid (1-40) Peptide Membrane Interactions: Aggregation Preventing Transmembrane Anchoring Versus Accelerated Surface Fibril Formation. *Journal of Molecular Biology* **335**, 1039-1049.

[45] Wood SJ, Maleeff B, Hart T, Wetzel R (1996) Physical, Morphological and Functional Differences between pH 5.8 and 7.4 Aggregates of the Alzheimer's Amyloid Peptide Aβ. *Journal of Molecular Biology* **256**, 870-877.

[46] Walsh DM, Hartley DM, Kusumoto Y, Fezoui Y, Condron MM, Lomakin A, Benedek GB, Selkoe DJ, Teplow DB (1999) Amyloid β-Protein Fibrillogenesis. STRUCTURE AND BIOLOGICAL ACTIVITY OF PROTOFIBRILLAR INTERMEDIATES. *Journal of Biological Chemistry* **274**, 25945-25952.

[47] Arispe N, Pollard HB, Rojas E (1993) Giant multilevel cation channels formed by Alzheimer disease amyloid beta-protein [A beta P-(1-40)] in bilayer membranes. *Proceedings of the National Academy of Sciences of the United States of America* **90**, 10573-10577.

[48] Arispe N, Diaz JC, Simakova O (2007) Aβ ion channels. Prospects for treating Alzheimer's disease with Aβ channel blockers. *Biochimica et Biophysica Acta (BBA) - Biomembranes* **1768**, 1952-1965.

[49] Capone R, Quiroz FG, Prangkio P, Saluja I, Sauer AM, Bautista MR, Turner RS, Yang J, Mayer M (2009) Amyloid-β-induced ion flux in artificial lipid bilayers and neuronal cells: resolving a controversy. *Neurotox Res* **16**, 1-13.

[50] Jang H, Zheng J, Nussinov R (2007) Models of beta-amyloid ion channels in the membrane suggest that channel formation in the bilayer is a dynamic process. *Biophys J* **93**, 1938-1949.

[51] Jang H, Zheng J, Lal R, Nussinov R (2008) New structures help the modeling of toxic amyloidß ion channels. *Trends in Biochemical Sciences* **33**, 91-100.

[52] Kremer JJ, Sklansky DJ, Murphy RM (2001) Profile of Changes in Lipid Bilayer Structure Caused by β-Amyloid Peptide. *Biochemistry* **40**, 8563-8571.

[53] Muller WE, Eckert GP, Scheuer K, Cairns NJ, Maras A, Gattaz WF (1998) Effects of beta-amyloid peptides on the fluidity of membranes from frontal and parietal lobes of human brain. High potencies of A beta 1-42 and A beta 1-43. *Amyloid* **5**, 10-15.

[54] Müller WE, Koch S, Eckert A, Hartmann H, Scheuer K (1995) β-amyloid peptide decreases membrane fluidity. *Brain Research* **674**, 133-136.

[55] Du H, Guo L, Yan S, Sosunov AA, McKhann GM, ShiDu Yan S (2010) Early deficits in synaptic mitochondria in an Alzheimer's disease mouse model. *Proceedings of the National Academy of Sciences* **107**, 18670-18675.

[56] McLaurin J, Chakrabartty A (1997) Characterization of the Interactions of Alzheimer beta-Amyloid Peptides with Phospholipid Membranes. *European Journal of Biochemistry* **245**, 355-363.

[57] Waschuk SA, Elton EA, Darabie AA, Fraser PE, McLaurin J (2001) Cellular Membrane Composition Defines Aβ -Lipid Interactions. *J. Biol. Chem.* **276**, 33561-33568.

[58] Kakio A, Yano Y, Takai D, Kuroda Y, Matsumoto O, Kozutsumi Y, Matsuzaki K (2004) Interaction between amyloid beta-protein aggregates and membranes. *Journal of Peptide Science* **10**, 612-621.

[59] Matsuzaki K (2007) Physicochemical interactions of amyloid β-peptide with lipid bilayers. *Biochimica et Biophysica Acta (BBA) - Biomembranes* **1768**, 1935-1942.

[60] Varnier A, Kermarrec F, Blesneac I, Moreau C, Liguori L, Lenormand J, Picollet-D'hahan N A Simple Method for the Reconstitution of Membrane Proteins into Giant Unilamellar Vesicles. *Journal of Membrane Biology* **233**, 85-92.

[61] Mecocci P, Cherubini A, Beal MF, Cecchetti R, Chionne F, Polidori MC, Romano G, Senin U (1996) Altered mitochondrial membrane fluidity in AD brain. *Neuroscience Letters* **207**, 129-132.

[62] Moreira PI, Santos MS, Moreno A, Oliveira C (2001) Amyloid beta-peptide promotes permeability transition pore in brain mitochondria. *Biosci Rep* **21**, 789-800.

[63] Moreira PI, Santos MS, Moreno A, Rego AC, Oliveira C (2002) Effect of amyloid beta-peptide on permeability transition pore: a comparative study. *J Neurosci Res* **69**, 257-267.

[64] Boldogh IR, Pon LA (2007) Mitochondria on the move. *Trends in Cell Biology* **17**, 502-510.

[65] Pizzo P, Pozzan T (2007) Mitochondria-endoplasmic reticulum choreography: structure and signaling dynamics. *Trends in Cell Biology* **17**, 511-517.

[66] Mannella CA, Buttle K, Rath BK, Marko M (1998) Electron microscopic tomography of rat-liver mitochondria and their interactions with the endoplasmic reticulum. *BioFactors* **8**, 225-228.

FIGURE LEGENDS

Fig. 1. Kinetics of Aβ_{42} fibril formation. Fibril formation was followed by the emission variation of *ThT linked to Aβ fibrils* ($\lambda_{ex}/\lambda_{em}$ *450/482 nm*) as a function of time. The ThT-Aβ complex specific fluorescence is given in relative units, *i. e.*, corresponding to the intensity of ThT in *Aβ buffer solution* (35 µM ThT, 11 µM Aβ_{42} peptide, 5 vol% DMSO, 0.5 mM HEPES, 0.5 mM EDTA, pH 7.4) divided by the intensity of ThT in *control solution* (35 µM ThT, 5 vol% DMSO, 0.5 mM HEPES, 0.5 mM EDTA, pH 7.4) at a given time. Each point has an error ≈ ± 12 %. One can notice that under the given conditions, fibril formation reaches saturation at sample "age" of about 40h. The dashed lines indicate the state of the two kinds of Aβ buffer solutions, "fresh" and "aged" Aβ buffer solutions (aged of about 1h, and of about 48h, respectively) used in this work for studying Aβ_{42} peptide interactions with model membranes.

Fig. 2. Effect of "aged" Aβ_{42} buffer solution on a GUV mimicking mitochondrial inner membrane (PC/PE/CL 60:30:10 mol/mol). See also **Supplementary Movie2_F2**. Local treatment (frames: 57 to 374s) with "aged" (48h after preparation) Aβ_{42} buffer solution (11 µM Aβ, 5 vol % DMSO, 0.5 mM HEPES, 0.5 mM EDTA, pH 7.4). GUV, made from PC/PE/CL 60:30:10 mol/mol in buffer 0.5 mM HEPES, 0.5 mM EDTA, at pH 7.4, as a model of the mitochondrial inner membrane leaflet exposed to cytoplasm pH. Peptide-induced increase of membrane thermal fluctuations indicating lowering of GUV global membrane tension. Vesicle shape changed from quasi-spherical (frame: 0s) to flaccid (frame: 390s). No local membrane deformation was observed. The vesicle preserved its integrity, no visible membrane damage occurred. T = 25°C.

Fig. 3. Test of the capacity of a GUV, pre-treated with "aged" Aβ_{42} buffer solution (shown in Fig. 2), to develop *cristae-like* morphology upon local acidification. See also **Supplementary Movie3_F3**. Adding locally 10 mM HCl (outside the GUV by a micropipette) initiated local membrane deformation (frame: 4.7s), followed by harsh rupture of the membrane zone affected by the acid (frame: 5.2s), and explosion of the GUV (frame: 6s). As soon as acid addition was stopped, the damaged membrane zone "re-healed", forming dense clumps (frame: 46.5s). No *cristae-like* morphology developed. T = 25°C, pH 7.4.

Fig. 4. Effect of "fresh" Aβ_{42} buffer solution on a GUV mimicking mitochondrial inner membrane (PC/PE/CL 60:30:10 mol/mol). See also **Supplementary Movie4_F4**. Local treatment (frames: 15.9 to 168.9s) with 'fresh' (1h after preparation) Aβ buffer solution (11 μM Aβ_{42}, 5 vol % DMSO, 0.5 mM HEPES, 0.5 mM EDTA, pH 7.4). GUV was made from PC/PE/CL 60:30:10 mol/mol in buffer 0.5 mM HEPES, 0.5 mM EDTA, at pH 7.4, as a model of the mitochondrial inner membrane leaflet facing cytoplasm pH. Vesicle size (frame: 0s) slightly decreased (frame: 193.3s). Like in the case of treatment with "aged" Aβ buffer solution (Fig. 5), no local membrane deformation was observed, the vesicle preserved its integrity, no visible membrane damage occurred. T = 25°C.

Fig. 5. Test of the capacity of a GUV, pre-treated with "fresh" Aβ_{42} buffer solution (shown in Fig. 4), to develop *cristae-like* morphology upon local acidification. See also **Supplementary Movie5_F5**. The local acidification (with up to 100 mM HCl) induced no visible effects to the GUV membrane, in contrast with the brutal rupture (achieved adding HCl solution of only 10 mM), observed in the case of acidification, after treatment with 'aged' Aβ buffer solution (**Fig. 3**). On the other hand, local acidification of GUV pre-treated with fresh Aβ buffer solution did not induce any local membrane invagination, no *cristae-like*

morphology was developed. This is in contrast with the case of local acidification of GUV not pre-treated with any Aβ, which does develop *cristae-like* morphology, as in **Supplementary-Fig. 4**, and [26], all other parameters being equal. T = 25°C, pH 7.4.

Fig. 6. Effect of "aged" Aβ_{42} (fibril containing) buffer solutions on lipid bilayer microscopic properties of LUVs mimicking mitochondrial inner membrane (PC/PE/CL 60:30:10 mol/mol). (A) and **(B)** - variation of the generalized polarization of Prodan, GP_{PRODAN} , and Laurdan, $GP_{LAURDAN}$ (1 fluorophore par 200 lipids); **(C)** DPH anisotropy, r_{DPH} (1 fluorophore par 500 lipids). **(left)** as a function of time, and, **(right)** as a function of the pH of the medium. Total peptide / lipid ratios (◊ – 0, □ – 1/100, Δ– 2/100, and, o – 4.4/100 mol/mol**.** T = 25°C. First, we followed during 4h the kinetics of Aβ_{42} interaction with LUVs**,** then we gradually lowered the pH of the Aβ_{42} -LUV samples by adding aliquots of acid solution**.**

Fig. 7. Test of the capacity of a GUV, pre-treated with "aged" reversed-Aβ_{42} (R-Aβ_{42}) buffer solution, to develop *cristae-like* morphology upon local acidification. See also **Supplementary Movie6_F7.** The GUV, upon subsequent local acidification (100 mM HCl), maintained its capacity to develop cristae-like tubular invaginations similar to those of the "healthy" (not pre-treated with any Aβ) GUV. However, the pH-induced tubular structures were thicker, shorter and less dynamic compared to those of "healthy" GUVs. T = 25°C, pH 7.4.

Fig. 8. Test of the capacity of a GUV, pre-treated with "fresh" reversed-Aβ_{42} (R-Aβ_{42}) buffer solution, to develop *cristae-like* morphology upon local acidification. See also

Supplementary Movie7_F8. Contrary to the case of pretreatment with the native "fresh" peptide, the GUV (upon local addition of 100 mM HCl) maintained its capacity to respond to the local pH gradient, thereby developing cristae-like tubular invaginations similar to those of the "healthy" (not pre-treated with any Aβ) GUV. However, in the case of pretreatment with **R-Aβ_{42}** , the initial tubular structures fragmented rapidly giving endocytic vesicles (non-reversible process). T = 25°C, pH 7.4.

FIGURES

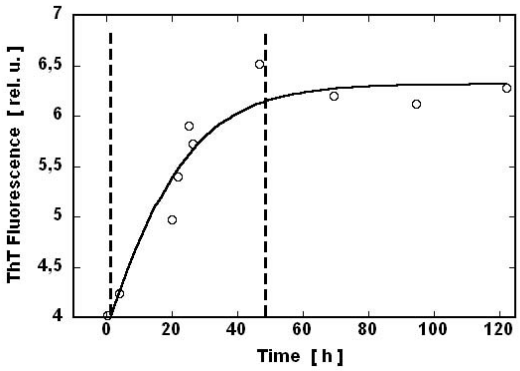

Fig. 1

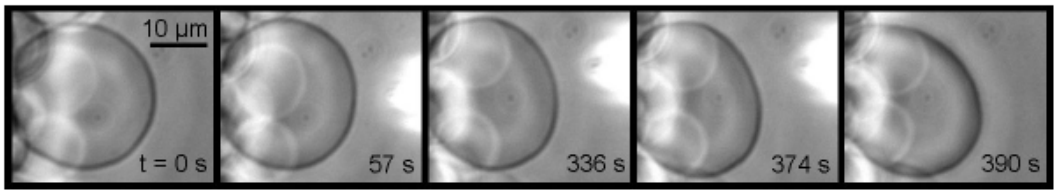

Fig. F2

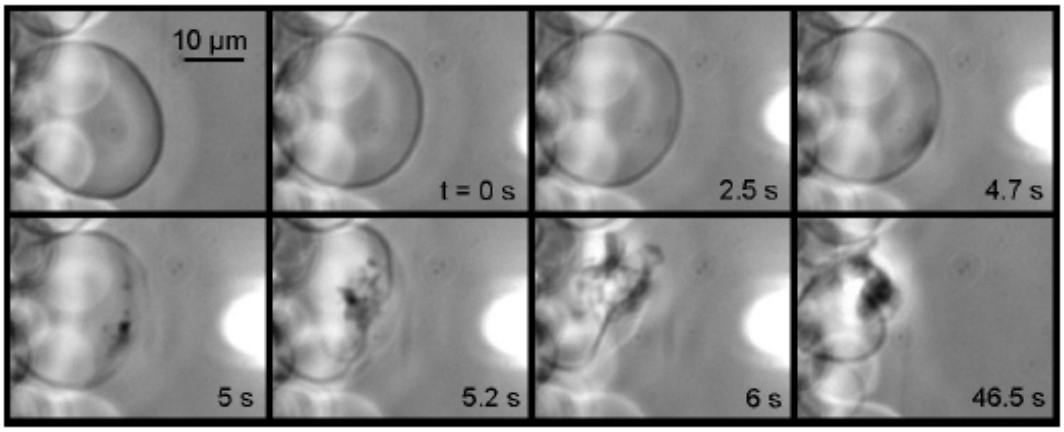

Fig. 3

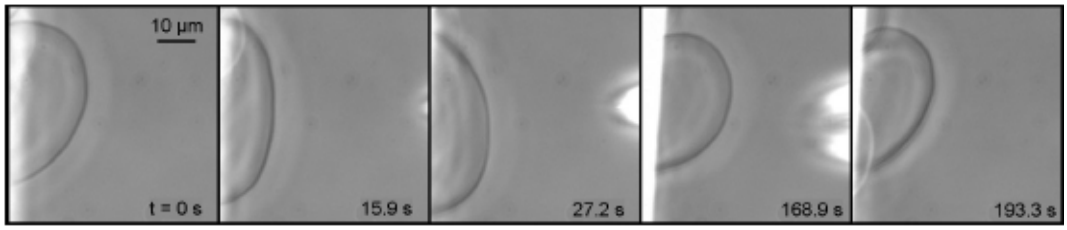

Fig. 4

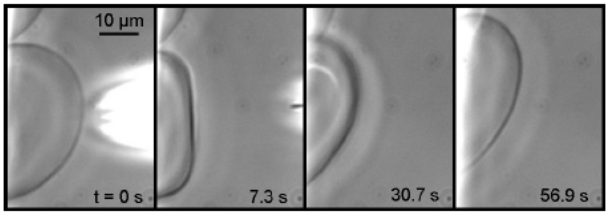

Fig. 5

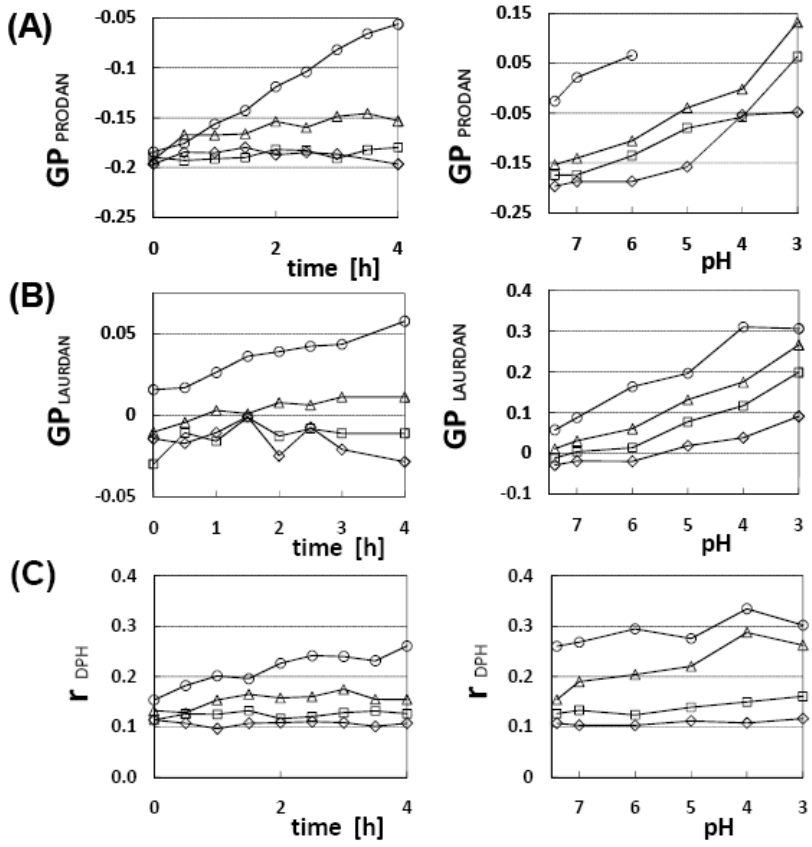

Fig. 6

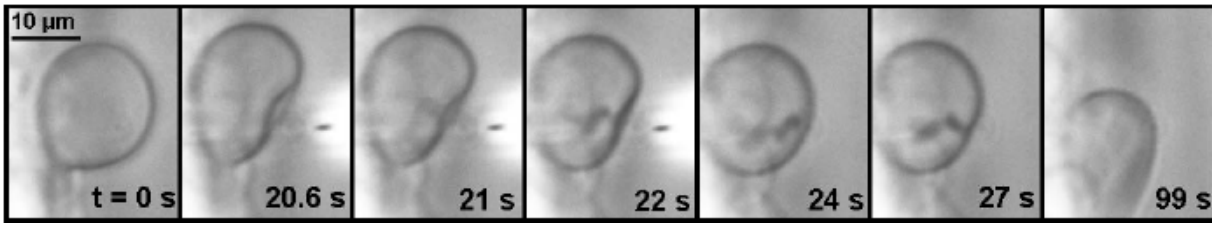
10 µm
t = 0 s
20.6 s
21 s
22 s
24 s
27 s
99 s

Fig. 7

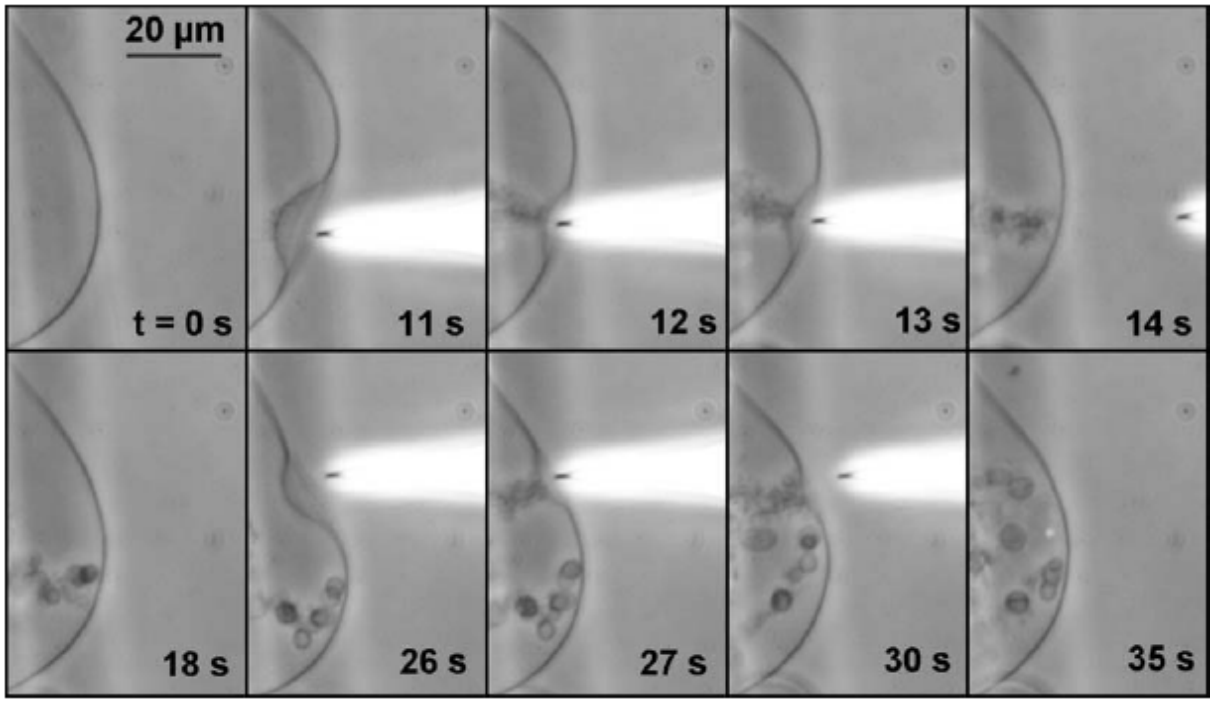
20 µm
t = 0 s
11 s
12 s
13 s
14 s
18 s
26 s
27 s
30 s
35 s

Fig. 8

SUPPLEMENTARY DATA

SUPPLEMENTARY - FIGURE LEGENDS:

Supplementary-Fig. 1.

(A) Conventional *transmission electron microscopy* (TEM) of a normal (healthy) mitochondrion - a typical text book image. This electron micrograph, *taken from Fawcett, A Textbook of Histology, Chapman and Hall, 12th edition, 1994*, *http://cellbio.utmb.edu/cellbio/mitoch1.htm*, shows the organization of the two membranes;

(B) TEM micrograph of Alzheimer's disease mitochondria. AD cybrid cells contained increased percentage of enlarged or swollen mitochondria, which had a pale matrix and *only a few remaining cristae*. Bar, 1 μm. Reprinted with permission from [18].

(C) Electron microscopy tomography images of a normal ("healthy") mitochondria. In living cells, mitochondria are usually tubular (1 to 2 μm long and 0.1 to 0.5 μm large) and interact with other cellular components, especially with the cytoskeleton and endoplasmic reticulum [64, 65]. Normally functioning mitochondria oscillate between **(a)** condensed and **(b)** orthodox state morphology, depending on their respiratory rate. Mitochondria performing maximum respiratory rate (in excess ADP and respiratory substrate) present condensed (matrix contracted) morphology (a). Their cristae are swollen cisterns or sacs connected to the peripheral part to the IM by narrow tubular segments (cristae junctions), **Fig. 1(C-a)** - the large white arrow. The cristae in orthodox (matrix expanded) morphology are narrow, flattened or almost tubular (b). OM diameter in (a) is 1.5 μm, in (b, lower) – 1.2 μm. (a) - (b) -

Supplementary-Fig. 2. Electron micrographs of mitochondria from a patient with AD and from a normal control patient. (a) - Polymorphism of mitochondria in a dendritic profile of a neuron of the globus pallidus in a patient with AD aged 62 years ; the majority of AD patient mitochondria were small and round or elongated; a substantial number of them showed *disruption of the cristae*. **(b) -** Mitochondria in the soma of a neuron of the globus pallidus in a control patient, aged 62 years. Reprinted with permission from [16].

Supplementary-Fig. 3. The neurotoxic action of Aβ involves generation of reactive oxygen species and disruption of cellular calcium homeostasis. Interactions of Aβ oligomers and Fe^{2+} or Cu^{+} generates H_2O_2. When Aβ aggregation occurs at the cell membrane, membrane-associated oxidative stress results in lipid peroxidation and the consequent generation of 4-hydroxynonenal (4HNE), a neurotoxic aldehyde that covalently modifies proteins on cysteine, lysine and histidine residues. Some of the proteins oxidatively modified by this Aβ-induced oxidative stress include membrane transporters (ion-motive ATPases, a glucose transporter and a glutamate transporter), receptors, GTP-binding proteins ("G proteins") and ion channels (VDCC, voltage-dependent chloride channel; NMDAR, *N*-methyl-d-aspartate receptor). Oxidative modifications of tau by 4HNE and other reactive oxygen species can promote its aggregation and may thereby induce the formation of neurofibrillary tangles. *Aβ can also cause mitochondrial oxidative stress and deregulation of Ca^{2+} homeostasis, resulting in impairment of the electron transport chain, increased production of superoxide anion radical and decreased production of ATP.* Superoxide is converted to H_2O_2 by the activity of superoxide dismutases (SOD) and superoxide can also interact with nitric oxide (NO) via nitric oxide synthase (NOS) to produce peroxynitrite (ONOO*). Interaction of H_2O_2 with Fe^{2+} or Cu^{+} generates the hydroxyl radical (OH*), a

highly reactive oxyradical and potent inducer of membrane-associated oxidative stress that contributes to the dysfunction of the ER. Reprinted with permission from [1].

Supplementary-Fig. 4. Design of a minimal model membrane system exhibiting dynamic cristae-like morphologies (a "healthy" GUV). See also **Supplementary-Movie1_SF4**. Modulation of local pH gradient at membrane level of a cardiolipin containing vesicle induces dynamic *cristae*-like membrane invaginations. GUV is made of PC / PE / CL 60:30:10 mol/mol in buffer at pH 8. The local delivery of HCl (100 mM pH 1.6 in the micropipette), which lowers the local pH down to about 5 to 4 at the membrane, is carried out by a micropipette (its position is pointed by the arrow in frame t=0 s).The induced membrane invagination (frame 22.8 s) is completely reversible (frames 38.7 to 66.4) as soon as the acid delivery is stopped. Deflated GUVs yield cristae-like morphology with large tubes and vesicular shape segments. Reprinted with permission from [26].

Supplementary-Fig. 5. Spectra of ThT total fluorescence for Aβ_{42} buffer solution at different times after solution preparation. Aliquots of peptide buffer solution were taken and mixed with aliquots of ThT solution (resulting sample: 35 μM ThT, 11 μM Aβ_{42} peptide, 5 vol % DMSO, 0.5 mM HEPES, 0.5 mM EDTA, pH 7.4) at 4h, 22h, 47h, and 95h, respectively. T = 25°C. The ThT fluorescence in the control solution is shown only for 4h (4h-control) as it was not changing significantly during the time of our experiment. It was as well practically the same as for the ThT fluorescence in the just buffer (no DMSO), data not shown, both being very low regarding the characteristic band for ThT *linked* to Aβ fibrils ($\lambda_{ex}/\lambda_{em}$ *450/482 nm*). The two vertical arrows indicate the two bands of ThT characteristic fluorescence corresponding respectively to the two states of ThT fluorophores eventually

presented in the sample: the *free* ThT ($\lambda_{ex}/\lambda_{em}$ *330/445 nm*) and, the ThT *linked* to Aβ fibrils ($\lambda_{ex}/\lambda_{em}$ *450/482 nm*).

SUPPLEMENTARY – MOVIE LEGENDS:

Movie1_SF4. Design of a minimal model membrane system exhibiting dynamic cristae-like morphologies (a "healthy" GUV), corresponding to **Supplementary-Fig. 4**.

Movie2_F2. Effect of "aged" Aβ_{42} buffer solution on a GUV mimicking mitochondrial inner membrane, corresponds to **Fig. 2** in the main text.

Movie3_F3. Test of the capacity of a GUV, pre-treated with "aged" Aβ_{42} buffer solution (shown in **Movie_F2**), to develop *cristae-like* morphology upon local acidification., corresponds to **Fig. 3** in the main text.

Movie4_F4. Effect of "fresh" Aβ_{42} buffer solution on a GUV mimicking mitochondrial inner membrane, corresponding to **Fig. 4** in the main text.

Movie5_F5. Test of the capacity of a GUV, pre-treated with "fresh" Aβ_{42} buffer solution (shown in **Movie_F4**), to develop *cristae-like* morphology upon local acidification. corresponding to **Fig. 5** in the main text.

Movie6_F7. Test of the capacity of a GUV, pre-treated with "aged" reversed-Aβ_{42} (R-Aβ_{42}) buffer solution, to develop *cristae-like* morphology upon local acidification, corresponding to **Fig. 7** in the main text.

Movie7_F8. Test of the capacity of a GUV, pre-treated with "fresh" reversed-Aβ_{42} (R-Aβ_{42}) buffer solution, to develop *cristae-like* morphology upon local acidification, corresponding to **Fig. 8** in the main text.

SUPPLEMENTARY – FIGURES:

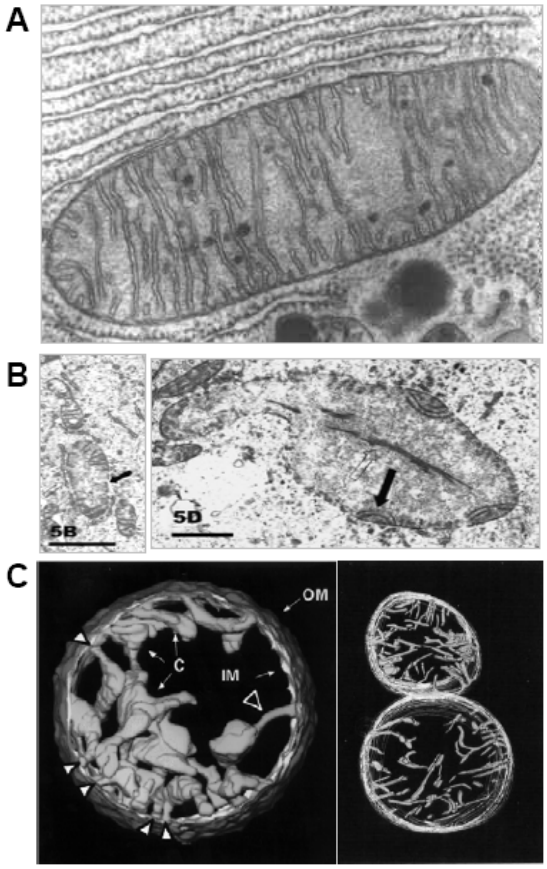

Supplementary-Fig. 1_A-B-C

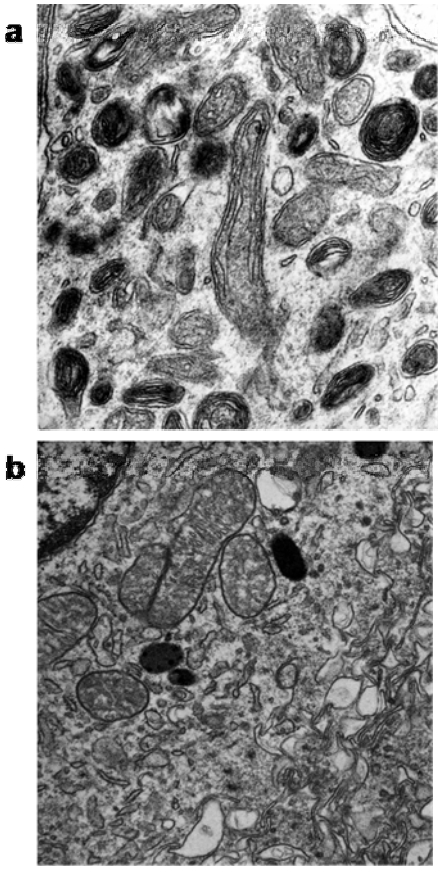

Supplementary-Fig. 2

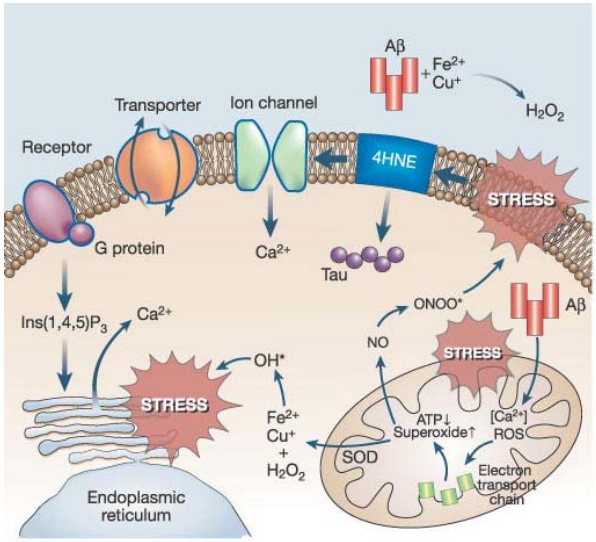

Supplementary-Fig. 3

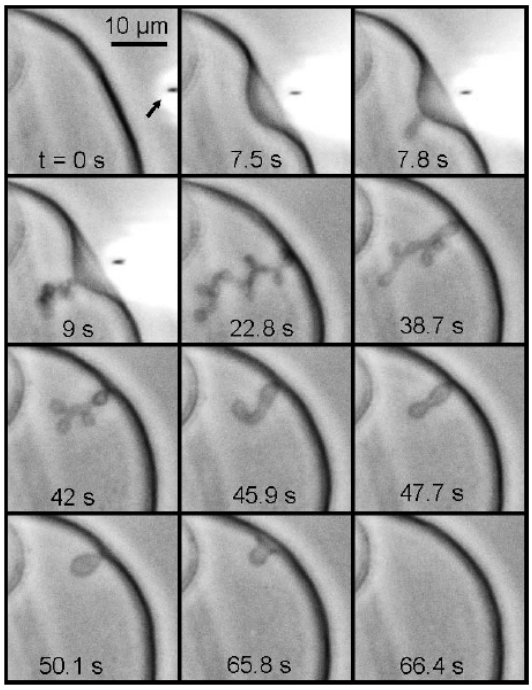

Supplementary-Fig. 4

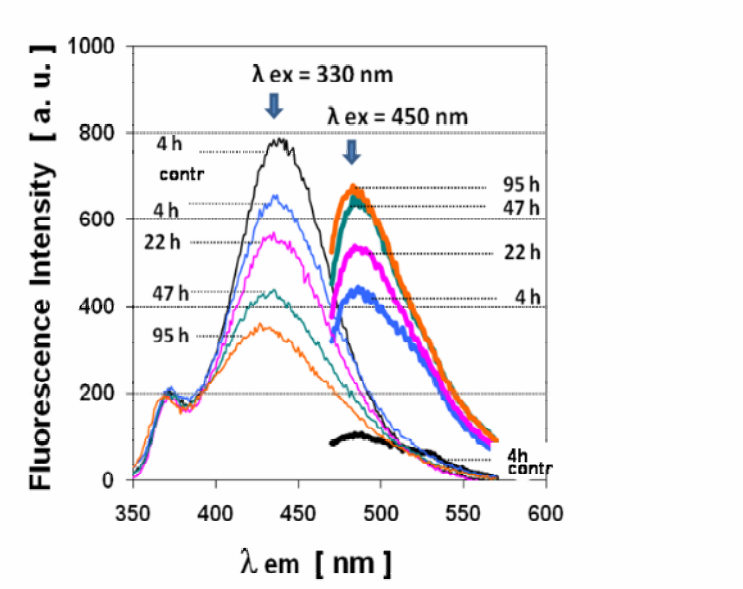

Supplementary-Fig. 5.